Interior Noise Predictions in the Preliminary Design
of the Large Civil Tiltrotor (LCTR2)

Ferdinand W. Grosveld
f.grosveld@nasa.gov
Structural Engineering Manager
Northrop Grumman
Hampton, Virginia, USA

Randolph H. Cabell
randolph.h.cabell@nasa.gov
Assistant Branch Head
NASA Langley Research Center
Hampton, Virginia, USA

D. Douglas Boyd, Jr.
d.d.boyd@nasa.gov
Aerospace Research Engineer
NASA Langley Research Center
Hampton, Virginia, USA

ABSTRACT

A prediction scheme was established to compute sound pressure levels in the interior of a simplified cabin model of the second generation Large Civil Tiltrotor (LCTR2) during cruise conditions, while being excited by turbulent boundary layer flow over the fuselage, or by tiltrotor blade loading and thickness noise. Finite element models of the cabin structure, interior acoustic space, and acoustically absorbent (poro-elastic) materials in the fuselage were generated and combined into a coupled structural-acoustic model. Fluctuating power spectral densities were computed according to the Efimtsov turbulent boundary layer excitation model. Noise associated with the tiltrotor blades was predicted in the time domain as fluctuating surface pressures and converted to power spectral densities at the fuselage skin finite element nodes. A hybrid finite element (FE) approach was used to compute the low frequency acoustic cabin response over the frequency range 6–141 Hz with a 1 Hz bandwidth, and the Statistical Energy Analysis (SEA) approach was used to predict the interior noise for the 125–8000 Hz one-third octave bands.

INTRODUCTION

The Large Civil Tiltrotor (LCTR) is a conceptual vehicle that was studied under the NASA Heavy Lift Systems Investigation as an economically competitive alternative to medium range regional airliners that could significantly relieve runway and terminal area congestion (Ref. 1). The tiltrotor design combines the speed, altitude and range of a turboprop airplane with the vertical lift capability of a helicopter thereby freeing up existing runways for use by larger and longer-range aircraft. A second-generation configuration of this vehicle, designated LCTR2, has a design goal to transport ninety passengers over a distance of 1800 km at a speed of 556 km/hr. An artist's rendering of the LCTR2 concept vehicle in forward flight is depicted in Figure 1. The LCTR2 was used as a representative vehicle design and mission under the NASA Fundamental Aeronautics Program (FAP) Subsonic Rotary Wing (SRW) project (Refs. 2 and 3). Several high risk areas have been identified for the LCTR2 configuration, such as the need for a high torque, low weight drive system and a high performance, structurally efficient rotor/wing system. Interior noise is expected to be distinctive due to the very low blade passage frequency of the four-bladed rotor (as low as 6.75 Hz during cruise conditions), the presence of a mid-wing gearbox and the turbulent boundary layer excitation during cruise flight conditions. When combined with the anticipated use of lightweight composite and sandwich materials in the fuselage sidewall, achieving acceptable interior noise levels in the LCTR2 may be challenging.

Previous efforts to predict the interior noise environment focused on turbulent boundary layer (TBL) excitation (Ref. 4) and the transmission loss characteristics of a notional LCTR2 sidewall structure (Ref. 5). The materials and lay-up of this notional sidewall were chosen to be similar to a Bombardier Dash-8 Q400 (Ref. 6) for which limited interior noise measurement data are available in the literature (Ref. 7).

Figure 1. Artist's rendering of the LCTR2 concept vehicle in forward flight.

The objective of the present study is to perform a preliminary assessment of the interior noise environment in the LCTR2 with this notional sidewall due to TBL excitation and blade passage-related noise from the tiltrotor (loading and thickness noise) at cruise conditions. The frequency range of interest extends from 6 Hz through 8000 Hz. To assess the acceptability of the predicted LCTR2 cabin noise levels, the maximum predicted levels are compared with interior noise measurements from the Q400.

LCTR2 DESIGN PARAMETERS

The LCTR2 is a conceptual design and no details of the fuselage sidewall, materials, cabin arrangement, overhead bins or interior trim have yet been established. To enable preliminary assessment of the interior noise for this study, a notional fuselage construction and geometry, including the skin, the ring frames, longitudinal stringers, bulkheads, floor, floor support beams, sidewall trim panels and noise control/thermal protection treatment were chosen with dimensions and material properties typical for an aircraft of that size and range. The specific aircraft used here was a proposed 90-passenger variant of the Bombardier Dash-8 Q400 (Ref. 8). A hypothetical layout of the LCTR2 cabin including four-abreast seating, lavatory, galley, and baggage areas is sketched in Figure 2. The relevant fuselage and flight parameters for the LCTR2 are listed in Table 1.
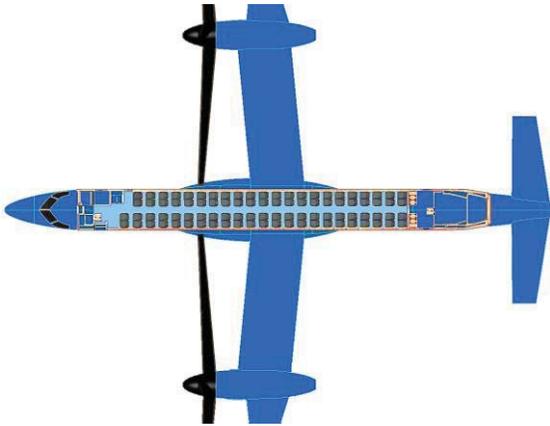

Figure 2. Sketch of a hypothetical LCTR2 90-passenger seating layout.

Table 1. Design parameters for the LCTR2.

Parameter		LCTR2
Passengers		90
Range	[km]	1800
Maximum cruise speed	[km/hr]	555.6
Maximum operating altitude	[m]	8534
Fuselage diameter	[m]	2.74
Maximum cabin width	[m]	2.56
Cabin length	[m]	21.84
Number blades	[-]	4
Blade passage frequency	[Hz]	6.75
RPM cruise	[rpm]	102
Rotor radius	[m]	9.91

PREDICTION SCHEME

A prediction scheme was established to compute sound pressure levels in the interior of the LCTR2 due to external TBL excitation and tiltrotor blade loading and thickness noise. The prediction scheme relied on finite element models of structural components and the cabin volume generated within MSC Patran (Ref. 9) that were then coupled together using the VA One vibro-acoustic analysis program (Ref. 10). Acoustically absorbing elements of the interior cabin were modeled within VA One as poro-elastic components. The external TBL excitation was represented by fluctuating power spectral densities derived using a semi-empirical TBL model. The properties of the TBL excitation were specified at nineteen axial sections of the fuselage to capture the evolution of the excitation in the flow direction as the boundary layer thickness changes. The tiltrotor noise from the blades was predicted in the time domain as fluctuating surface pressures (FSP) and converted to power spectral densities at the fuselage skin finite element nodes by a Fast Fourier Transform (FFT).

The specific prediction scheme varied with the frequency range of the prediction. From 6-141 Hz, the cabin noise was predicted using a deterministic, narrowband (1 Hz) analysis. A statistical approach was used to predict noise in third-octave bands from 125-8000 Hz. Note that 141 Hz is the upper frequency of the 125 Hz one-third octave band, thereby allowing comparison between the low and high frequency analyses in the overlapping 125 Hz one-third octave band.

At low frequencies, where acoustic and structural wavelengths are long compared to the dimensions of the sidewall structure and interior cabin, the vibro-acoustic response is deterministic and can be adequately described by a deterministic approach such as finite element analysis. However, at higher frequencies and associated shorter wavelengths, the required size of the finite elements becomes so small that the deterministic approach becomes impractical. This is not only due to a growth in the model size, but also because it is exceedingly difficult to model important variations in the structure that become significant at high frequencies, such as material property variations, dimensional variations, and random variations due to manufacturing. Therefore at high frequencies a stochastic approach, such as Statistical Energy Analysis (SEA), is used to obtain the space averaged vibro-acoustic response. The boundary between the two analyses is not precise, but for the present work the finite element mesh density defines the upper frequency limit for deterministic analysis. A modal analysis of the fuselage structure was performed in MSC Nastran (Ref. 11) and the modal parameters and the mode shape deflection information were imported into the VA One program. Rigid-boundary acoustic modes were computed in VA One and were coupled with the in-vacuo modes of the structure by a velocity continuity boundary condition at their interfaces. Although the structural components and the acoustic space are modeled using finite elements, it is computationally efficient to use a stochastic representation for the sound radiated outward from the fuselage into the surrounding fluid. This is accomplished within VA One by using a hybrid method (Ref. 10), which combines Finite Elements (FE) with Statistical Energy Analysis (SEA) subsystems. Specifically, a stochastic semi-infinite fluid (SIF) is attached to the externally radiating face of the FE structural model as a radiation impedance to capture energy propagating away from the fuselage structure. In subsequent discussions, this low frequency model will be referred to as a

hybrid FE/SEA model. The high frequency model will be referred to simply as an SEA model.

CABIN SIMULATION MODELS

This section describes details of the prediction models, including the generation and application of external excitations. More information on geometric details and material properties is available in Ref. 4.

Low Frequency Hybrid FE/SEA Model

The low frequency vibro-acoustic simulation model includes FE models of the structure and acoustic cavities, Poro-Elastic Finite Element Method (PEM) subsystems and a semi-infinite fluid (SIF). Pressurization effects were not included in the hybrid FE/SEA model, since the effects were assumed to be negligible in the low frequency range where global modes of the structure dominate.

Structural Finite Element Models

The cabin structural FE model represents the fuselage as a floor-equipped, stiffened cylinder. The model includes the skin, longitudinal stringers, ring frames, floor, floor support beams, and bulkheads. Specifics of the sidewall geometry were defined using geometry and material information of the Bombardier Dash-8 Q400 fuselage section described in Ref. 6. The fuselage is stiffened by thirty-nine evenly spaced ring frames and sixty-eight evenly spaced longitudinal stringers (longerons) bordering a total of 2584 fuselage sidewall bays. The ring frame spacing is 0.58 m while the distance between stringers along the circumference is 0.124 m. The skin in each bay area between the ring frames and the longerons is represented by a matrix of two Quad4 elements in the circumferential direction and four Quad4 elements in the axial direction.

The ring frames have a "U"-shaped cross-section while the longitudinal stringers have a "Z"-shaped cross-section (Ref. 6). The floor support beams have a "U"-shaped cross section as well. The perimeter and area of the cross sections were computed, along with the cross-sectional property parameters such as the moments of inertia, the polar moment, torsional constant, distance from shear center to centroid and the shear stiffness factors.

The skin of the fuselage consists of 1.6 mm-thick aluminum with a surface density of 4.35 kg/m^2. The ring frames and the longitudinal stringers for the baseline configuration are also made of aluminum.

The floor is supported by thirty-nine horizontal floor beams with the same 0.58 m spacing as the ring frames. Each floor section between horizontal supports was assumed to be a honeycomb sandwich structure. Unidirectional, 0.71 mm thick S-2 glass reinforced epoxy facings were selected as face sheets and were assumed to be bonded to an aramid honeycomb core in a construction similar to other

typical aircraft flooring panels (Ref. 12). The mechanical material properties of the face sheets and the 8.92 mm thick honeycomb core, along with thickness and orientation values, were entered as laminated composites in the MSC Patran modeler. The total thickness of the stacking sequence is 10.34 mm with a total density of 377 kg/m^3. Each floor section was modeled with sixteen Quad4 elements along its width and four Quad4 elements between the supports. All beams are represented by Beam2 elements. An isometric view of the basic finite element model without the bulkheads is shown in Figure 3.
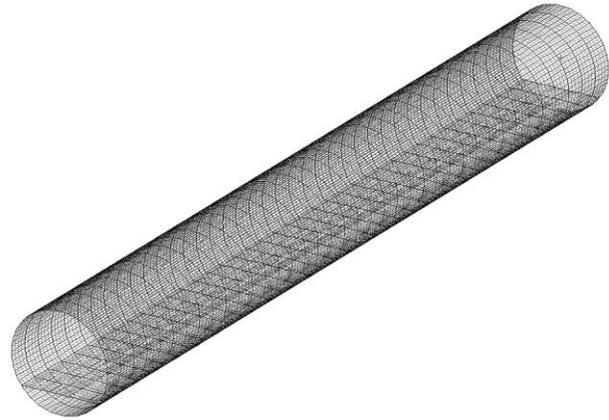

Figure 3. Basic finite element model of the fuselage skin, ring frames, longitudinal stringers, floor, and floor support beams.

Poro-Elastic Finite Element Method (PEM) Models

PEM models were used for the fuselage sidewall trim, the floor coverings, the seats, and the overhead bins to more accurately represent their poro-elastic properties. The PEM solver in VA One is based on a finite element implementation of the poro-elastic, elastic and acoustic equations of motion and is used to generate the modal impedance matrix coupled to the structural and acoustic FE subsystems. A PEM subsystem may encompass foam material, fiber material, elastic solid structures, limp structures or acoustic fluids.

The fuselage sidewall trim consisted of a thin airgap, a porous absorption material and a trim panel. The honeycomb polymer trim panels, typical for a Q400 aircraft (Ref. 13), were located 81 mm from the fuselage skin. The trim panels were 3 mm thick with a surface density of 0.765 kg/m^2 and an estimated loss factor of 0.02. The porous absorption material between the trim panel and the sidewall was assumed to be 80 mm thick melamine foam layer with a loss factor of 0.17. The diffuse field absorption coefficient of the melamine foam is indicated by the red curve in Figure 4. A thin airgap (1 mm) was included in the model to signify the separation between the foam and the fuselage skin. The thin airgap and the melamine foam were represented in the PEM model with solid elements, while shell elements were used for the trim panel.

The floor covering consisted of a 3 mm thick floor surface (shell elements in the PEM model), with an estimated loss factor of 0.1, on top of a fiber poro-elastic material modeled with solid elements.
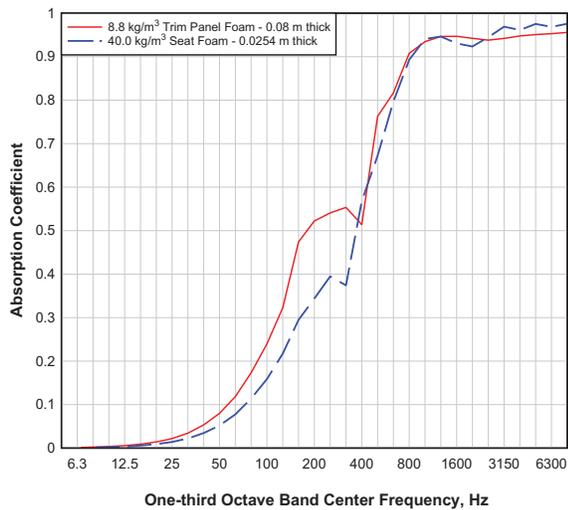

Figure 4. Diffuse field absorption coefficients of the seat foam and the 0.08 m thick acoustic foam used in the trim.

The space in the structural finite element model above the floor was meshed with solid elements. A rudimentary representation for the seats and the overhead bins was obtained by carving out their occupied volumes from the finite element mesh above the floor. The resulting solid elements corresponding to the seats and bins were then converted to PEM subsystems within the VA One program. The diffuse field absorption coefficient of a 25.4 mm thick sample of the foam typically used in seats is indicated by the dashed blue curve in Figure 4. The overhead bins were assumed to be stowed and were assigned equivalent isotropic solid material properties.

An isometric view of the PEM models for the sidewall trim, the floor covering, the seats and the overhead bins is presented in Figure 5. A cross-sectional view is shown in Figure 6.
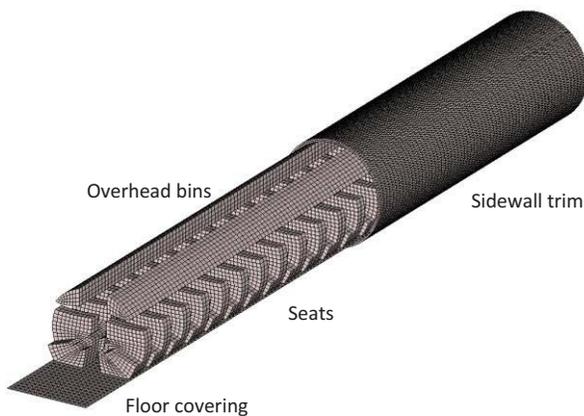

Figure 5. Porous Elastic Finite Element Method (PEM) models for the seats, overhead bins, floor covering and interior trim.

Four linear elements per wavelength of the propagating waves in the porous materials are recommended for accurate PEM analysis allowing a frequency analysis range up to and including the 125 Hz one-third octave band with borderline qualifications for the seat foam in the 125 Hz band.
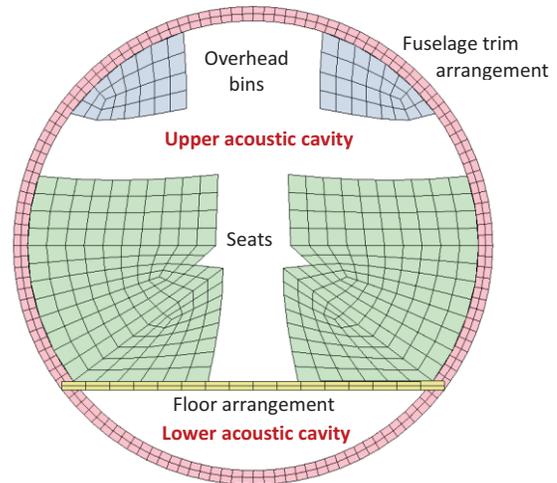

Figure 6. Cross-sectional view of the PEM models for the seats, overhead bins, floor covering and interior trim.

Acoustic Finite Element Models

The acoustic upper cavity in Figure 6 was created by subtracting the finite elements corresponding to the seats, overhead bins, floor and sidewall trim from the total cabin volume above the floor. This acoustic upper cavity was assigned properties of air for the pressurized aircraft cabin (Table 2) and divided in two parts: the volume forward of the tiltrotor plane and the volume aft of the tiltrotor plane. Figure 7 shows the forward and aft acoustic upper cavities relative to the tiltrotor plane. The solid elements in the meshed volume below the floor were also assigned properties of air for the pressurized aircraft.

Table 2. LCTR2 and Q400 cruise flight conditions.

Parameter			LCTR2 Outside	Cabin	Q400 Outside
Altitude	h	[m]	8534	2438	7620
Temperature	T	[°C]	-40.7	20.0	-34.53
Pressure	P	[Pa]	32934	75266	37600
Density	ρ	[kg/m^3]	0.4931	0.897	0.5489
Speed of sound	c	[m/s]	305.8	343.3	309.7
Kinematic viscosity	υ	[m^2/s]	$3.05 \, 10^{-5}$	$2.02 \, 10^{-5}$	$2.8 \, 10^{-5}$
Flow velocity	U_0	[m/s]	154.3		185.3
Mach number	M_c	[-]	0.505		0.60

High Frequency SEA Model

At the higher frequencies the modal density and modal overlap in the structure and acoustic space increase significantly and a statistical description of the modes in the subsystems becomes more useful. Less detail is required and only the average response of the subsystem is predicted. The porous noise control treatments are weakly coupled to the structure and mainly provide sound absorption.
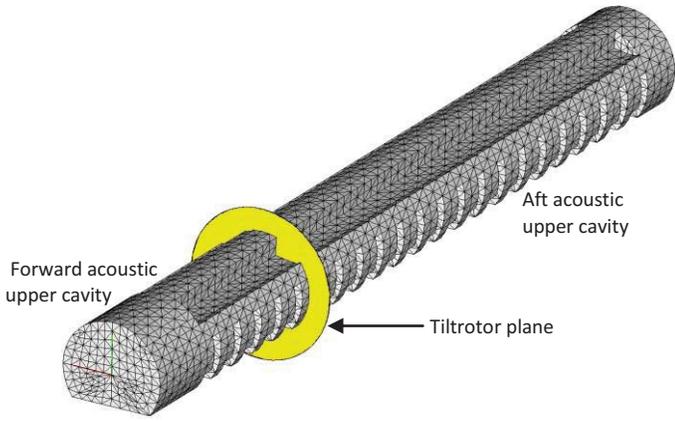
4

Figure 7. The forward and aft acoustic cavities above the floor relative to the tiltrotor plane.

Structural SEA Model

The fuselage structure and floor were divided into fifty-seven SEA subsystems, as shown in Figure 8. The axial length of each subsystem was twice the separation between ring frames of the fuselage. Thus, the floor was divided into nineteen subsystems, as were the fuselage sections above and below the floor. This allows computation of the energy flow and structural response at nineteen subsystems along the fuselage of the cabin. The fuselage skin, the longitudinal stringers and the ring frames were represented by ribbed plate subsystems with as input the skin material and mechanical properties, the beam material properties, the moments of inertia, the torsional constants, the cross-sectional areas, the locations of the shear center relative to the neutral axis of the section, the centroid offsets and the beam spacing. The floor and the supporting floor beams were modeled in a similar manner. Pressurization, the difference between internal and external pressures, was used in VA One to define the in-plane tensions and resulting geometric stiffness of the bay skin panels between the ring frames and the longitudinal stringers.
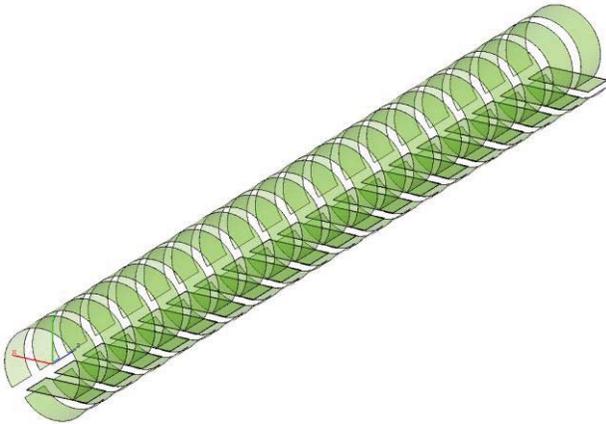

Figure 8. Fifty-seven 1.16 m wide structural subsystems (shrunken for clarity), including the floor panels and the curved ribbed skin sections above and below the floor.

Acoustic SEA Model

Similar to the structural model, the interior acoustic space was divided into nineteen sections above the floor and nineteen sections below the floor. The resulting thirty-eight acoustic subsystems are shown in Figure 9; the tiltrotor plane corresponds to the black circumference in the figure. The combined effect of the floor covering, trim panels, and seats was represented using a frequency dependent effective acoustic absorption in the cabin. The absorption was taken as the lower bound of the average of experimental acoustic absorption data available for high-speed propeller driven aircraft (Refs. 14 and 15).
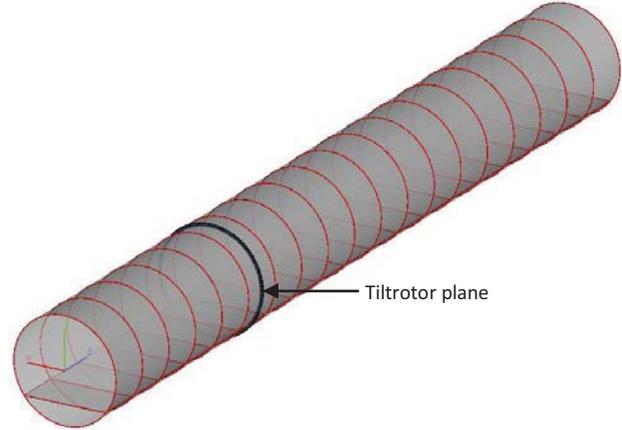

Figure 9. Thirty-eight acoustic cavity sections relative to the tiltrotor plane.

EXCITATION MECHANISMS

Turbulent Boundary Layer Excitation

The turbulent boundary layer noise was modeled as a fluctuating pressure spectrum in the acoustic prediction code VA One (Ref. 10). The turbulent boundary layer thickness δ at distance x_0 from the nose of the tiltrotor vehicle was computed from the relation

$$\delta = 0.37 \frac{x_0}{Re^{0.2}} \tag{1}$$

where Re is the Reynolds number, which is defined by

$$Re = \frac{U_0 x_0}{\upsilon} \tag{2}$$

The free stream velocity U_0, the kinematic viscosity υ and the properties of air at cruise altitude are listed in Table 2. The Efimtsov turbulent boundary layer semi-empirical model is available in VA One but was computed outside the program to achieve better parameter control, after which the excitation power spectral densities were imported into VA One.

5

The power spectral density Φ_E of the turbulent boundary layer pressure fluctuations according to the empirical model by Efimtsov is given by (Refs. 17, 18 and 19)

$$\Phi_E = 2\pi U_\tau^3 \rho^2 \delta \frac{\alpha\beta}{\left(1+8a^3 S_t^2\right)^{1/3} + \alpha\beta Re_\tau \left(S_t Re_\tau\right)^{10/3}} \quad (3)$$

where $U_\tau = U_0 (c_f/2)^{0.5} = (\tau/\rho)^{0.5}$ is the friction velocity, $\alpha = 0.01$, $\beta = [1+(3000/Re_\tau)^3]^{1/3}$, $S_t = \omega\delta/U_\tau$ is the Strouhal number, and $Re_\tau = U_\tau\delta/\upsilon$ is the Reynolds number.

The spatial correlation function R_F for a free stream velocity at $M<0.75$ with convection velocity U_c is given by

$$R_F\left(\varepsilon,\eta,\omega\right) = \exp\left\{-\frac{|\varepsilon|}{\delta}\left[\left(\frac{a_1 S_t}{U_c/U_l}\right)^2 + \frac{a_2^2}{S_t^2 + \left(a_2/a_3\right)^2}\right]^{0.5} - \right.$$
$$\left. -\frac{|\eta|}{\delta}\left[\left(\frac{a_4 S_t}{U_c/U_l}\right)^2 + \frac{a_5^2}{S_t^2 + \left(a_5/a_6\right)^2}\right]^{0.5} \frac{i\varepsilon\omega}{U_c}\right\} \quad (4)$$

where the ratio of velocities is defined by

$$\frac{U_c}{U_l} = a_8 S_t^{0.2}\left[\frac{1+\left(a_9 S_t\right)^2}{1+\left(a_{10} S_t\right)^4}\right]^{0.1} \quad (5)$$

with coefficient values $a_1 = 0.1$; $a_2 = 72.8$; $a_3 = 1.54$; $a_4 = 0.77$; $a_5 = 548$; $a_6 = 13.5$; $a_7 = 5.66$; $a_8 = 9.55$; $a_9 = 0.000638$; $a_{10} = 0.00398$.

The convection wavenumber $k(f)$ in the direction of the flow is ω/U_c and equals zero in the direction perpendicular to the flow. For Mach numbers lower than 0.75 the Efimtsov boundary layer decay coefficients c_x and c_y are given by (Ref. 17)

$$c_{x,y} = \frac{1}{\delta}\left[\left(\frac{a_{1,4} S_t}{U_c/U_l}\right)^2 + \frac{a_{2,5}^2}{S_t^2 + \left(a_{2,5}/a_{3,6}\right)^2}\right]^{0.5}$$
$$\left(\frac{\omega^2}{U_c^2} + \frac{7.11}{\left(0.37 X_0 R_e^{-0.2}\right)^2}\right)^{-0.5} \quad (6)$$

Power spectral densities due to the Efimtsov boundary layer excitation were computed for each of the nineteen fuselage sidewall sections to account for the increase in boundary layer thickness as a function of the distance from the nose of the LCTR2 vehicle.

Tiltrotor Blade Harmonic Noise

The comprehensive rotorcraft analysis code CAMRAD II (Ref. 20) was used in this work to determine the trim state of the tiltrotor vehicle given the flight condition in Table 2 with a flight path angle of zero degrees (level flight). The tiltrotor nacelles were in airplane mode, with the tiltrotors acting as two large prop-rotors. For this case, the control settings for the governor (effectively the rotor blade collective pitch), the longitudinal rotor blade cyclic input, and the pitch attitude of the vehicle were adjusted to achieve a symmetric trim state of the vehicle. Here, a symmetric trim is achieved when the vertical force, the horizontal force, and the pitch moment of the entire vehicle is zero.

Because the trim state of the free flight vehicle is primarily concerned with determining the net forces and moments on the vehicle, it is not necessary to compute the rotor blade aerodynamics at a high azimuthal resolution. The trim is performed with a 15-degree azimuthal time step for the rotor blades.

Aerodynamic Modeling

Within CAMRAD II, the rotor blades are modeled with lifting lines coupled to a prescribed wake geometry model. The local blade aerodynamics were computed on fifteen aerodynamic panels along the span of each blade. The lift, drag, and pitch moment aerodynamic coefficients for the rotor blade sections use airfoil tables which are a function of angle of attack and Mach number. Airfoil table corrections are included to account for items such as yawed flow, sweep, static stall, etc. The LCTR2 blades are modeled as rigid blades as elastic blade effects are expected to be of secondary importance in the current study.

The fuselage aerodynamics are also modeled using separate aerodynamic tables for lift, drag, pitch moment, horizontal tail lift, and horizontal tail drag. The lift, drag, and pitch moment tables are functions of angle of attack, Mach number, and the wing flap angle. The horizontal tail aerodynamic tables are functions of angle of attack, Mach number, and elevator angle.

For acoustic calculations, high resolution aerodynamics are needed. However, because the trim state was determined at a low azimuthal resolution, an additional step was necessary. This additional step in CAMRAD II is known as the "post-trim". The "post-trim" calculation performs an additional iteration at a high azimuthal resolution.

The final results to be used in the acoustic calculations are a high resolution description of the lift and drag forces distributed along the blade lifting line, as well as three displacement and three Euler angle distributions along the blade lifting line.

Fluctuating Pressure Time History Computations

The Ffowcs Williams and Hawkings (FW-H) solver, PSU-WOPWOP (Ref. 22), is used for the acoustic analysis. The acoustic solver requires information about the blade

geometry as well as any loading on the blade for a noise calculation.

Airfoil - Because CAMRAD II uses a lifting line analysis with airfoil tables, there is no requirement for an airfoil profile. However, the acoustic analysis needs an airfoil profile for the thickness noise calculations. Therefore, the LCTR2 rotor blade is modeled by National Advisory Committee for Aerodynamics (NACA) sections using a thickness that matches the LCTR2 blade thicknesses. For the acoustic calculations, the inboard blade section is modeled as a NACA 0028 airfoil and linearly tapers to a NACA 0008 section at the blade tip. Other geometric parameters, such as built-in twist, precone, etc. are already included in the blade geometric description from CAMRAD II.

Loading - The loading applied in the acoustic analysis is the normal and chordwise force vector distribution along the span of each blade, determined by the post-trim in CAMRAD II.

PSU-WOPWOP includes a capability to use lifting line-type data through a compact chordwise model of the FW-H equations. Using PSU-WOPWOP, the acoustic pressures due to the thickness and loading were computed at 2685 nodes of the structural finite element model at the locations where the thirty-nine ring frames and the sixty-eight longitudinal stringers overlap. Both rotors were included in the computations.

Scattering and surface reflections – In the PSU-WOPWOP computations no account was made for fuselage acoustic scattering, reflections, etc. That is, each node on the fuselage was treated as if it were in the free field. Although future PSU-WOPWOP predictions will include scattering, in the current study a simple reflection correction was applied based on empirical data from various propeller configurations for vertical and short take-off and landing (V/STOL) aircraft (Ref. 23). The empirical reflection correction factors described in this Aerospace Information Report (AIR) (Ref. 23) were scaled to the tiltrotor diameter and the distance forward and aft of the tiltrotor plane. The surface reflection corrections, shown in Figure 10 as function of the number of frames away from the tiltrotor plane, were applied to the acoustic pressures at the frame nodes of the fuselage finite element model.

Fluctuating Surface Pressure Excitation

A contour plot of the PSU-WOPWOP predicted time history data with the tiltrotor blades close to the fuselage surface is shown in Figure 11. These fluctuating external pressures produce a deterministic force on the modes of the fuselage structure. The 0.148224 s length of the time history data was chosen to cover the time between two blades passing a fixed point and was divided into 128 time steps of 0.001158 s each. The time data were imported into VA One where a Fast Fourier Transform (FFT) was performed. The chosen time step resulted in a maximum analysis (Nyquist)

frequency of 432 Hz and the total time record yielded an FFT bandwidth of approximately 6.75 Hz. Since the excitation is deterministic and one exact period of the blade passage signal is used in the analysis no window was applied to the time signal. The frequency domain FSP data at the 2685 nodes were converted to power spectral densities and were interpolated for all nodes on the fuselage shell by specifying a distance within which each node is associated with the data of the closest node in the imported file.
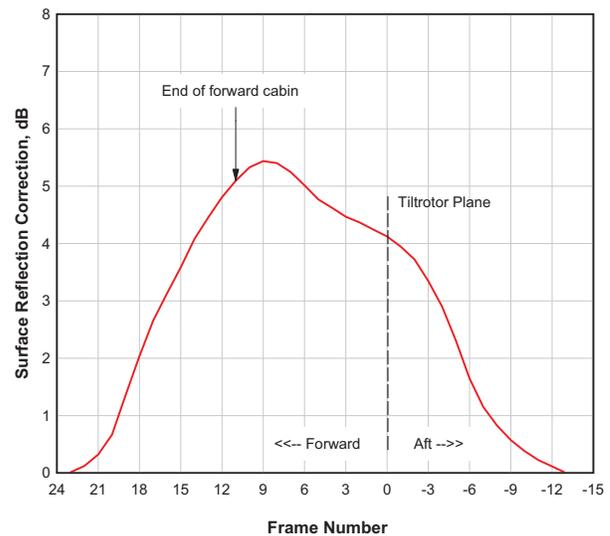

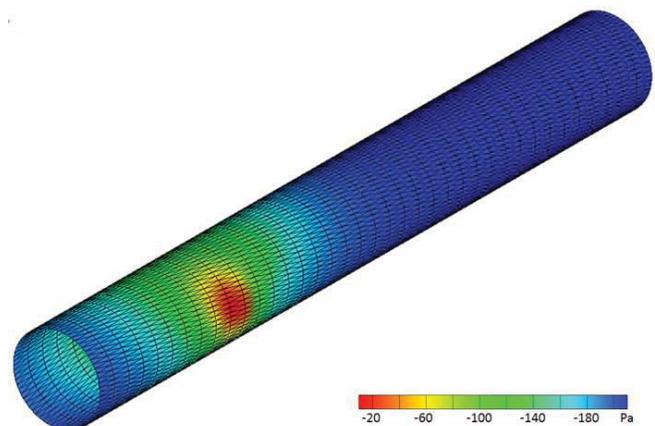**Figure 10. Surface reflection corrections as function of frame number from the tiltrotor plane.**

Figure 11. Contour plot of PSU-WOPWOP predicted time history data corrected for surface reflections at nodes on the finite element shell.

ANALYSES

The hybrid FE/SEA model considered excitation due to both the TBL and the tiltrotor blade passage frequency (BPF)-related noise. The SEA model only considered the TBL excitation, since it was determined that at higher frequencies the blade-related noise was sufficiently below the TBL excitation to be ignored.

Low Frequency Hybrid FE/SEA Analysis

Structural Modal Response

The in-vacuo structural modal response of the fuselage model, including the fuselage skin, ring frames, longitudinal stringers, the floor and the floor supports, was computed using MSC Nastran 2010 (Ref. 11). Simply supported boundary conditions were assumed at the aft bulkhead location and the forward flight deck entrance. Future analyses will include more realistic boundary conditions to represent the fuselage being supported by the wings at the wing box interface. The structural modal analysis results were then imported into VA One. A default 1% structural damping loss factor was assumed. The lowest structural mode of the fuselage occurred at 9.07 Hz. The mode is a first order axial mode as it has no nodal lines between the aft bulkhead and the front flight deck access. The number of structural modes in the one-third octave bands with center frequencies 5–160 Hz is listed in Table 3.

Acoustic Modal Response

The acoustic modes in the cavities above and below the floor were computed by a modal analysis in VA One. The lowest acoustic mode, in the axial direction, was predicted to occur at 5.7 Hz and is a first-order axial mode having one nodal line in the center with the highest interior sound pressure levels occurring at the bulkhead and the forward flight deck wall. The first cross-sectional acoustic mode at 73.8 Hz has a vertical nodal line and the highest responses occur at the two opposite fuselage sidewalls. This acoustic mode may efficiently couple to structural circumferential mode(s). The number of acoustic modes computed in each one-third octave band is listed in Table 3.

Table 3. Number of acoustic and structural modes in the one-third octave bands 5–160 Hz.

One-third octave band center frequency [Hz]	Acoustic modes #	Structural modes #
5	1	-
6.3	-	-
8	-	-
10	-	2
12.5	1	2
16	1	4
20	-	9
25	1	17
31.5	1	19
40	2	29
50	2	31
63	3	42
80	20	73
100	25	93
125	21	129
160	60	183

Cabin Interior Noise Predictions

VA One computes the cabin sound pressure levels in the low frequency region by applying the appropriate excitation, coupling the in-vacuo structural modes, the rigid-boundary acoustic modal parameters and the PEM modal impedance matrix, and accounting for energy propagating away from the structure by including a radiation impedance. The resulting interior noise is reported here as the spatially averaged sound pressure level (SPL) over the cabin volumes forward and aft of the tiltrotor plane.

Turbulent Boundary Layer Excitation - The predicted forward and aft cabin interior sound pressure levels due to TBL excitation are shown in Figure 12 along with the averaged sound pressure levels for the entire cabin. Except for the 6-9 Hz frequencies the averaged sound pressure levels in the aft part of the cabin are generally higher than the averaged levels in the forward cabin, which is related to the coupling of the acoustic and structural modes, and the higher TBL excitation towards the rear of the cabin.
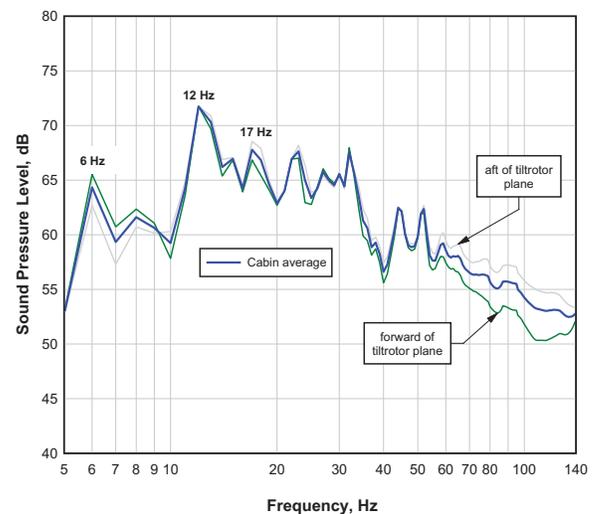

Figure 12. Spatial average of the narrowband (1 Hz) LCTR2 cabin sound pressure levels forward and aft of the tiltrotor plane for TBL excitation predicted with the low frequency hybrid FE/SEA analysis.

At low frequencies the interior cabin sound pressure level variations are determined by the coupled acoustic and structural modal responses. The natural frequencies of the structural and acoustic modes below 20 Hz are tabulated in Table 4. The first, second, and third axial acoustic modes occur at 5.75 Hz, 11.6 Hz and 17.6 Hz, respectively and are the only acoustic cabin modes below 20 Hz. The acoustic mode number indicates the number of nodal lines in the response. Eleven structural modes were identified below 20 Hz and their axial mode numbers are included in Table 4 as well. The structural mode number indicates the number of anti-nodes or the number of nodal lines plus one.

The acoustic and structural modes will couple most efficiently if they have similar spatial characteristics and their modal frequencies are close. As an example, the third-order axial acoustic resonance at 17.6 Hz (Figure 13)

couples well with the second-order structural modes at 17.3 Hz (Figure 14) and 18.7 Hz (Figure 15) due to the spatial characteristics of the acoustic modal pressures and the structural modal displacements. Both the acoustic and the structural modes have a nodal line in the center and maximum responses on either side. The resulting distribution of the predicted sound pressure levels in the cabin at 17 Hz is shown in Figure 16 and is similar to the variations in the acoustic modal response. Peak interior sound pressure levels coincide with the maximum acoustic modal response at approximately one-third and two-third of the length of the cabin. Sound pressure level variations inside the cabin are as high as 16 dB. The predicted space averaged interior sound pressure levels result in a peak at 17 Hz as shown in Figure 12. Similarly the peaks at 6 Hz and 12 Hz in Figure 12 are associated with the acoustic modes at 5.75 Hz and 11.6 Hz. In fact, all the peaks up to 70 Hz in the sound pressure level predictions of Figure 12 are attributed to the coupling of axial acoustic modes with axial structural modes. As frequency increases, progressively higher-order axial modes join the overall modal response. The first cross-sectional acoustic mode was computed at 73.8 Hz and is characterized by a vertical nodal line in the tiltrotor plane cross-section. The 73.8 Hz frequency is in the 80 Hz one-third octave band which contains 73 structural and 20 acoustic resonant modes (Table 3). Several non-resonant modes participate in the modal response of the 80 Hz one-third octave band as well. A cross-sectional mode with a horizontal nodal line was calculated at 128.9 Hz in the 125 Hz one-third octave band. The number of acoustic and structural resonances in the 125 Hz band equals 21 and 129 respectively (Table 3) and the number of modes participating has grown so large that the individual cross-sectional modes only have a minor contribution to the global cabin noise and the SEA method is more appropriate for interior noise predictions. However, these cross-sectional modes still may cause local hotspots of sound, especially close to the fuselage sidewall where they may efficiently couple to circumferential structural modes.

Tiltrotor Blade Noise Excitation –The sound pressure levels predicted by the hybrid FE/SEA model for the blade passage frequency at 6.75 Hz and the first twelve harmonics are shown in Figure 17. The predicted levels due to the TBL excitation are included to serve as a reference.

Similar to the TBL excitation, the tiltrotor blade passage frequency results are affected by the acoustic and structural modal behavior of the cabin. At the blade passage frequency the sound pressure level averaged over the forward cabin is almost 96 dB while the average level in the aft cabin is 10 dB lower. Up to 50 Hz the harmonic noise associated with the blade passage frequency is higher than the turbulent boundary layer noise. At 87.7 Hz the broadband turbulent boundary layer related sound pressure level in the aft cabin is more than 10 dB higher than the twelfth harmonic of the BPF. This difference was deemed sufficient to consider the harmonic noise to be completely masked by the TBL noise. Although the difference between TBL and BPF-related noise

was only 6 dB in the aft cabin, the sound pressure levels are low enough that they will not adversely effect human response. These results suggest that harmonics greater than twelve times the BPF do not need to be considered for interior noise analysis.

Table 4. Frequencies of acoustic and structural modes below 20 Hz.

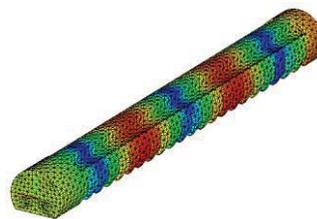| Acoustic mode [Hz]	Axial mode order	Structural mode [Hz]	Axial mode order
5.75	First		
		9.07	First
		9.20	First
11.6	Second	11.4	First
		11.5	First
		14.3	Second
		14.8	Second
		15.3	First
17.6	Third	17.3	Second
		18.5	First
		18.7	Second
		19.4	Third

Figure 13. Third-order axial acoustic resonance at 17.6 Hz.
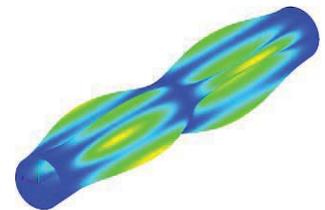

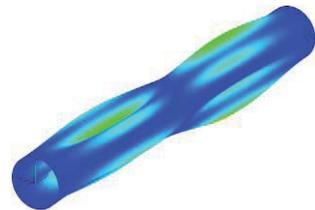**Figure 14. Second-order axial structural resonance at 17.3 Hz.**

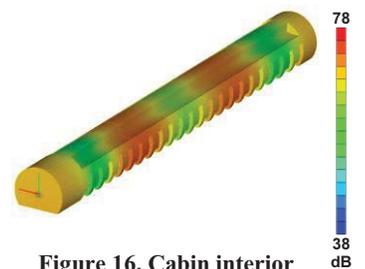**Figure 15. Second-order axial structural resonance at 18.7 Hz.**

Figure 16. Cabin interior sound pressure level distribution at 17 Hz.

High Frequency SEA Analysis

A high frequency SEA analysis was performed for the structural and acoustic subsystems excited by TBL only. The modal density in the acoustic space above the floor was estimated to exceed approximately one mode per Hertz in the 125 Hz and higher bands. The hybrid FE results demonstrated that BPF-related noise was not important at these higher frequencies. A semi infinite fluid (SIF)

representing an unbounded exterior acoustic space was connected to the nineteen curved structural subsystems of the upper as well as the lower fuselage sections to serve as an acoustic radiation impedance. The curved shell of the fuselage was exposed to a pressure differential of 42.3 kPa to create representative in-plane tensions and resulting geometric stiffness of the fuselage skin panels.
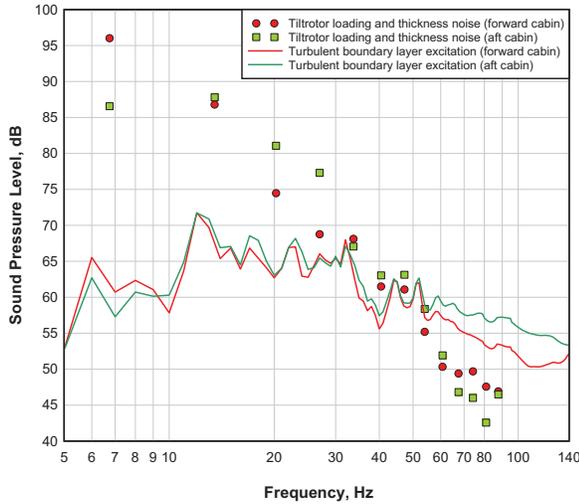

Figure 17. LCTR2 cabin sound pressure levels averaged over the forward or aft cabin due to tiltrotor noise and turbulent boundary layer excitation predicted with the low frequency hybrid FE analysis.

Sound pressure levels for each interior acoustic subsystem along with their averaged values are plotted in Figure 18. The highest interior sound pressure levels are in the aft-most cabin subsystem where the turbulent boundary layer thickness is at a maximum.
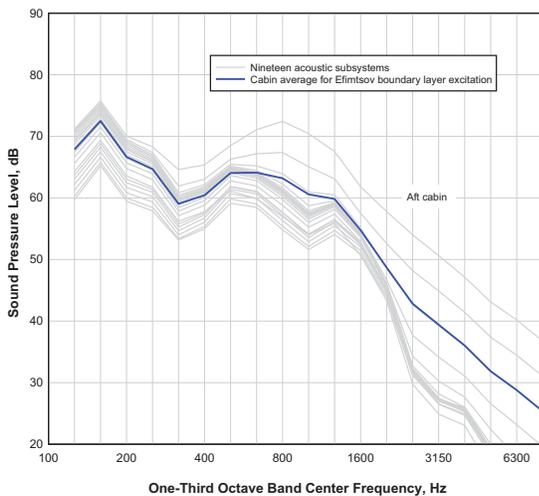

Figure 18. SEA predicted one-third octave band LCTR2 subsystem sound pressure levels and their average for the turbulent boundary layer excitation.

LCTR2 Analysis Results for the Consolidated Frequency Range

The narrowband predictions from the hybrid FE/SEA model shown in Figure 12 were converted to one-third octave bands and are plotted in Figure 19 along with the high frequency SEA predicted cabin averaged sound pressure levels. The predictions for the hybrid FE/SEA and SEA models due to TBL excitation differ by less than 1 dB in the 125 Hz one-third octave band. However, this good agreement may be fortuitous as the interior sound pressure levels are averaged over the cabin, and several parameters like loss factors, acoustic absorption values, boundary conditions, trim treatment and others are modeled differently in the low and high frequency approaches. Also, pressurization was not modeled for the hybrid FE approach but was included in the SEA analysis.
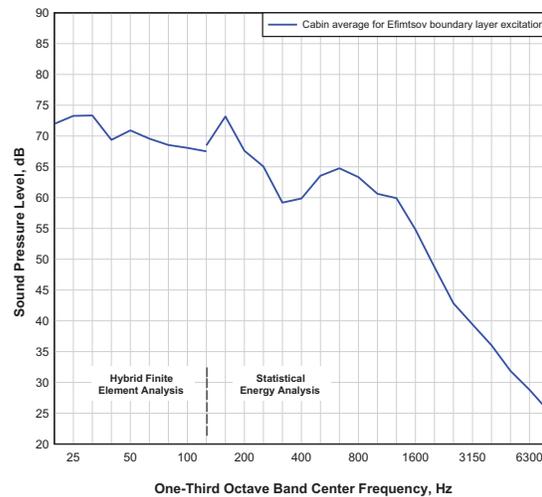

Figure 19. Averaged one-third octave band LCTR2 sound pressure levels predicted for the Efimtsov model with the hybrid FE analysis (20-125 Hz) and with SEA (125-8000 Hz).

Predictions Compared with Measurements in the Bombardier Q400

Although no controlled experimental acoustic data are available to validate the LCTR2 predictions, a comparison is made here with interior noise data from a Dash-8 Q400 turboprop (Ref. 13) as a preliminary assessment of passenger acceptability of the predicted LCTR2 interior noise. The interior noise measurements in Ref. 13 were made in the front cabin of a Q400 at cruise altitude during level flight. Cruise conditions for the Q400 are summarized in Table 2. During these measurements, the active noise and vibration suppression system in the Q400 was operational.

The maximum measured SPL in the forward cabin of the Q400 is indicated by the dashed green curve in Figure 20 in terms of one-third octave band levels. The level peaks at the propeller blade passage frequency near 80 Hz and its harmonics in the 160 and 315 Hz one-third octave bands.
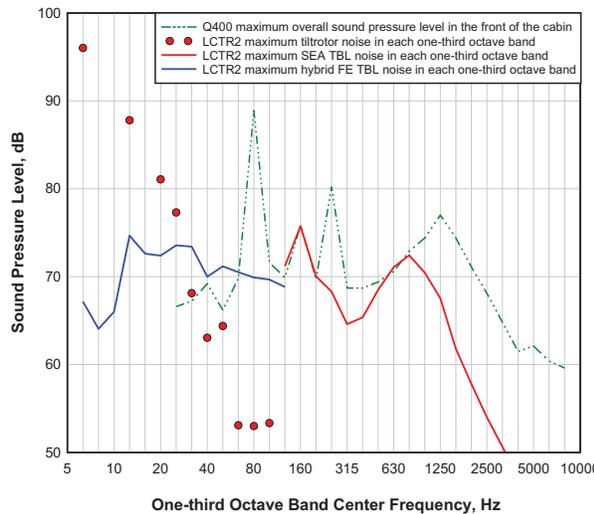
Figure 20. Maximum one-third octave band LCTR2 cabin sound pressure levels for the tiltrotor noise excitation, and hybrid FE and SEA predicted turbulent boundary layer excitation compared with the highest measured overall level at a location in the forward cabin of the Q400.

Superimposed on the Q400 measurements are predicted interior noise levels in the LCTR2 due to various sources. The blue curve shows spatially averaged TBL-induced noise at low frequencies; while the red circles indicate blade passage-related noise levels. The red curve shows TBL-induced noise at high frequencies, as predicted using the SEA model. In each case, the worst-case predicted noise levels are shown.

The predicted noise level in the LCTR2 at the tiltrotor blade passage frequency and its first harmonic is higher than or equal to the level at the Q400 blade passage frequency. However, the LCTR2 frequencies are below the audible frequency range (< 20 Hz) and at the indicated levels are unlikely to annoy passengers, although they may still impact vibrational comfort of the passengers.

The low frequency (< 125 Hz) TBL prediction exceeds the measured Q400 spectrum by 9 dB at 25 Hz (Figure 20). However, there are many possible sources of inaccuracy in the prediction as well as uncertainties in the measured data. These include material property assumptions, detailed flight-test conditions, and the precise measurement location and the proximity of that location to the sidewall trim and seat surfaces.

The higher frequency prediction of noise due to the TBL excitation is generally equal or lower than the measured Q400 levels. This is in part due to the lower LCTR2 cruise speed (Mach 0.51 versus Mach 0.60 for the Q400) and higher LCTR2 cruise altitude (8534 m versus 7620 m for the Q400). It may also be due to the fact that the measured data in the figure were taken from the forward cabin, where TBL-induced noise is generally lower than in the aft cabin. In addition to the uncertainty sources mentioned above, there are additional possible contributes to the measured noise level in this frequency range, such as the environmental control system, and passenger noise.

In summary, for the Q400 fuselage sidewall and layout adopted as the baseline for the notional LCTR2, the interior noise levels above the 63 Hz one-third octave band due to blade-passage noise and due to TBL excitation were predicted to be less than the noise measured in a Q400 turboprop aircraft. Tonal noise associated with the tiltrotor blades was predicted to be below the measured Q400 noise associated with the rotor blades, except for the LCTR2 predictions at the 6.75 Hz blade passage frequency and its first harmonic at 13.5 Hz. Although sound at these frequencies is inaudible (< 20 Hz) it may still impact the passengers or crew or otherwise adversely affect human perception and acceptability, and further study may be warranted.

SUMMARY

Interior sound pressure levels in the cabin of a notional Large Civil Tiltrotor (LCTR2) due to turbulent boundary layer flow over the fuselage and blade passage-related noise during cruise flight conditions were computed. Structural and acoustic finite element models were created and combined with models of poro-elastic elements such as the seats, overhead bins, fuselage trim, and floor coverings. An Efimtsov turbulent boundary layer excitation model was used to specify exterior excitation levels of nineteen segments of the fuselage in order to capture variation of the excitation spectra with distance from the nose of the vehicle. The tiltrotor noise from the blades was predicted in the time domain as fluctuating surface pressures (FSP) and converted to power spectral densities at the fuselage skin finite element nodes by a Fast Fourier Transform (FFT). Cabin interior sound pressure levels were predicted employing a narrowband (1 Hz) hybrid Finite Element (FE) analysis for the low frequencies (6-141 Hz) and a Statistical Energy Analysis (SEA) method for the high frequency one-third octave bands (125-8000 Hz). It is shown that the interior sound pressure level distribution in the low frequencies is governed by interactions between individual structural and acoustic modes. Peak sound pressure levels occurred at the same locations as the maxima in the acoustic modal response.

Predicted interior noise levels were compared with the highest one-third octave band levels measured in the front cabin of a Bombardier Q400 during cruise conditions. Blade passage-related noise for the third harmonic and above in the LCTR2 was predicted to be lower than measured levels in the Q400. Although the first two harmonics were predicted to be higher in the LCTR2, sound at these frequencies (6.75 Hz and 13.5 Hz) is generally inaudible, although it may still adversely affect passengers and crew as a source of vibration, and warrants further study. LCTR2 predicted turbulent boundary layer associated noise below 125 Hz was determined not to affect human perception, due to its low

levels or, below 20 Hz, not being audible. Interior noise levels above the 125 Hz one-third octave band due to the turbulent boundary layer excitation were predicted at lower levels than the noise measured in the Q400 turboprop aircraft. The procedure described here will be used to evaluate the interior noise impact of more advanced fuselage designs and newer materials.

REFERENCES

1. Johnson, W., Yamauchi, G.K., and Watts, M.E.: NASA Heavy Lift Rotorcraft Systems Investigation. NASA TP-2005-213467, September 2005.
2. Acree, C.W., Yeo, H., and Sinsay, J.D.: Performance Optimization of the NASA Large Civil Tiltrotor. International Powered Lift Conference, London, UK, July 2008; also NASA TM-2008-215359, June 2008.
3. Acree, C.W. Jr.: Integration of Rotor Aerodynamic Optimization with the Conceptual Design of a Large Civil Tiltrotor, NASA Ames, ARC-E-DAA-TN1176, January 2010.
4. Grosveld, Ferdinand W.: Large Civil Tiltrotor (LCTR2) Interior Noise Predictions due to Turbulent Boundary Layer Excitation. NASA/TM 2013-000000, March 2013.
5. Grosveld, Ferdinand W. and Cabell, Randolph, H.: Preliminary assessment of the interior noise environment in the Large Civil Tiltrotor (LCTR2). nc11_129, Proceedings of Noise-Con 2011, Portland, Oregon, USA, 25-27 July 2011.
6. Gardonio, P. and Gonzalez Diaz, C.: Bombardier Dash-8 Q400 Fuselage Section with Five Decentralized Velocity Feedback Control Units. ISVR Technical Memorandum 983. Institute of Sound and Vibration Research, Southampton, UK, January 2009.
7. Tubbs, Randy L.: NIOSH Health Hazard Evaluation Report HETA 2002-0354-2931. Horizon Air. Seattle, Washington. February 2004.
8. Aviation International News: Bombardier considers stretch variant for Q400. Paris Air Show. Air Transport and Cargo Aircraft. June 2009.
9. MSC Patran 2012. MSC Software Corporation, Santa Ana, California, 2012.
10. VA One 2011 User's Guide. ESI Group North America, December 2011.
11. MSC Nastran 2010.1.1. MSC Software Corporation, Santa Ana, California, 2012.
12. Gillfloor 4017T Light Weight Aircraft Flooring Panel. M.C. Gill Corporation, El Monte, CA, March 2001.
13. Alujević, Neven: Smart double panel with decentralised active damping units for the control of sound transmission. Institute of Sound and Vibration Research, University of Southampton, England, August 2008. (http://eprints.soton.ac.uk)
14. Wilby, J.F., Rennison, D.C. and Wilby, E.G.: Noise Control Predictions for High-Speed, Propeller-Driven Aircraft. AIAA-80-0999, AIAA 6th Aeroacoustics Conference, Hartford, Connecticut, 4-6 June 1980.
15. Rennison, D.C., Wilby, J.F., Marsh, A.H., and Wilby, E.G.: Interior Noise Control Prediction Study for High-Speed, Propeller-Driven Aircraft. NASA Contractor Report 159200, NASA Langley Research Center, Hampton, Virginia, September 1979.
16. Cockburn, J.A., Robertson J.E.: Vibration Response of Spacecraft Shrouds to In-flight Fluctuating Pressures. *Journal of Sound and Vibration*, 1974, 33(4), pp. 399-425.
17. Efimtsov, B.M.: Characteristics of the field of turbulent wall pressure fluctuations at large Reynolds numbers. *Soviet Physics Acoustics*, 1982, 28, pp. 289-292.
18. Rackl, R., and Weston, A.: Modeling of Turbulent Boundary Layer Surface Pressure Fluctuation Auto and Cross Spectra – Verification and Adjustments Based on TU-144LL Data. NASA/CR-2005-213938, December 2005.
19. Miller, T.S., Gallman, J.M., and Moeller, M.J.: Review of Turbulent Boundary-Layer Models for Acoustic Analysis. *AIAA Journal of Aircraft*, Vol. 49, No. 6, November-December 2012, pp. 1739-1754.DOI: 10.2514/1.C031405
20. Johnson, W.: CAMRAD II: Comprehensive Analytical Model of Rotorcraft Aerodynamics and Dynamics (Release 4.7). Volumes 1-9, Johnson Aeronautics, 2008.
21. Acree, C.W., Johnson, W.: Aeroelastic Stability of the LCTR2 Tiltrotor. AHS Technical Specialists' Meeting, Dallas, TX, October 15-17, 2008.
22. Hennes, C., Lopes, L., Shirey, J., Erwin, J., Brentner, K.S.: PSU-WOPWOP 3.3.3 User's Guide, Pennsylvania State University, May 4, 2009.
23. Society of Automotive Engineers - SAE Technical Standards: Prediction Procedure for Near-Field and Far-Field Propeller Noise. SAE International – Aerospace Information Reports, SAE AIR 1407-1977 (Reaffirmed: April 1991).